solved x-ray spectrometry have shown that the final core state is in reasonable agreement with the prediction of the one-dimensional hydrocode. They thus imply a reasonably high level of symmetry in the shell implosion. In addition, we report the independent estimate of the final core ρR product by two separate techniques; this is a diagnostic development which should find many applications in future experiments.

2.C Stress-Induced Birefringence in the Nearly Athermal Glass LHG-8

Recent[1] theoretical estimates of the target illumination uniformity required for direct-drive experiments have assumed azimuthally symmetric beam profiles. In order to match those assumptions as closely as possible in experiments on the OMEGA laser system, a study was initiated to identify sources of azimuthal beam asymmetry. This program has improved our understanding of stress-induced birefringence in rods of the nearly athermal glass LHG-8 used in OMEGA. Nearly athermal glasses are so called because the change in index, n, with temperature is approximately opposite to the change in the product of $(n - 1)$ times the coefficient of expansion. Such glasses do not exhibit the usual large change in optical path with a change in temperature. However, they still show birefringence due to stresses created by radially non-uniform pumping. In what follows, only rod geometries with azimuthal symmetry are considered. End effects are also ignored.

A rod with an azimuthally symmetric temperature profile behaves as a waveplate with principal axes in the radial and tangential directions. Using Quelle's formalism,[2] it is possible to calculate the change in optical path for radial and tangential polarizations in a thermally stressed rod from those of an isothermal rod. The needed parameters are Young's modulus, Poisson's ratio, the coefficient of thermal expansion, the change in index with temperature, the photoelastic constants, and the temperature profile. If all that is wanted is path difference between radial and tangential polarizations, i.e., the birefringence, only the difference between the photoelastic constants is needed. The only parameter that is usually unknown is the temperature profile. Based on confidence established in one-dimensional simulations of the stored energy and heat deposition in active-mirror amplifiers, we approximated the temperature profile in 40-, 64-, and 90-mm-diameter rod amplifiers as a constant times the small-signal gain profiles. This was particularly convenient as the rod radial gain profiles are routinely measured. The one-Cartesian-dimension pumping simulations assume that the deposited heat is due to Nd ion absorption from 340 to 900 nm, and to undoped glass absorption from 340 to 700 nm. There are several Nd contributions that must be counted in the heating calculation. They are:

1) the so-called quantum defect, which is the energy difference between the absorbing Nd energy level and the $4F_{3/2}$ upper lasing level. The cascade to the upper lasing level is assumed to be phonon-dominated (little fluorescence);
2) cooperative relaxation among adjacent excited and unexcited Nd ions; and

3) phonon-assisted decay from the 4I levels to the ground state after fluorescence from the $4F_{3/2}$ level.

For the 0.54 wt-% doped sample of LHG-8 pumped by the flashlamps used in the rod amplifiers, the simulations predict that, on the spatial average, at the time of peak gain, for every joule of stored energy in the form of inversion, there should be approximately 1.9 joules of deposited heat, primarily from the quantum defect. This is a lower bound as UV and IR glass absorption has been ignored. If this number is used to calculate the stress-induced birefringence in the aforementioned rods, small amounts of birefringence are found.

To measure the active birefringence, the amplifiers were placed on a translation stage between crossed polarizers. A collimated He-Ne probe with a Gaussian beam intensity distribution having approximately 1-mm FWHM was carefully aligned parallel with the rod edge. The wavelength dispersion of stress birefringence was assumed to be small. A large-area photodiode intercepted the transmitted light. The output of the photodiode was monitored on an oscilloscope and data was taken by a sampling digital voltmeter accurately timed to sample at the fluorescence or gain peak of the rod under test. Prior to each shot, the transmission of the rod was measured with the polarizers parallel. This allowed the normalized transmission at gain maximum to be calculated, and from it, the birefringence. A minimum of two measurements were made at each of approximately eight radial locations in every rod. The rods were cooled by a 50%/50% solution of ethylene glycol and water. A strip chart recorder was connected to the photodiode output to be sure rethermalization was complete before the next measurement. A scan started at the edge of the rod and proceeded inward until the measured birefringence fell below 0.5 nm/cm.

One 40-mm rod, two 64-mm rods, and one 90-mm rod were tested. The smaller rods all had the same Nd-doping of 0.54 wt-% while the 90-mm rod was doped at 0.39 wt-%. The 40-mm rod was pumped at 75% of the bank energy of the others. The two 64-mm rods were identical except that #530B had undergone over 500 system shots before it was removed for birefringence testing.

The measured birefringence in nm/cm versus distance from the rod edge is plotted for three of the rods in Fig. 19. Also shown for the three rods is the least squares best fit that was made by varying the constant of proportionality between the measured stored energy profile and the assumed temperature profile used in Quelle's model. As expected, the 40-mm rod exhibited the largest temperature change per unit radius, and exhibited the greatest birefringence. The 90-mm rod exhibited the least temperature change, and the least birefringence. Each cross represents one data point. Since three shots at the most were taken at a single location, no statistics were generated and no error bars were assigned in the vertical direction. The radial position was always known to within $\pm$ 0.5 mm and corresponds approximately to the size of the cross in the horizontal direction.

Figure 20 compares the active birefringence of the two 64-mm rods

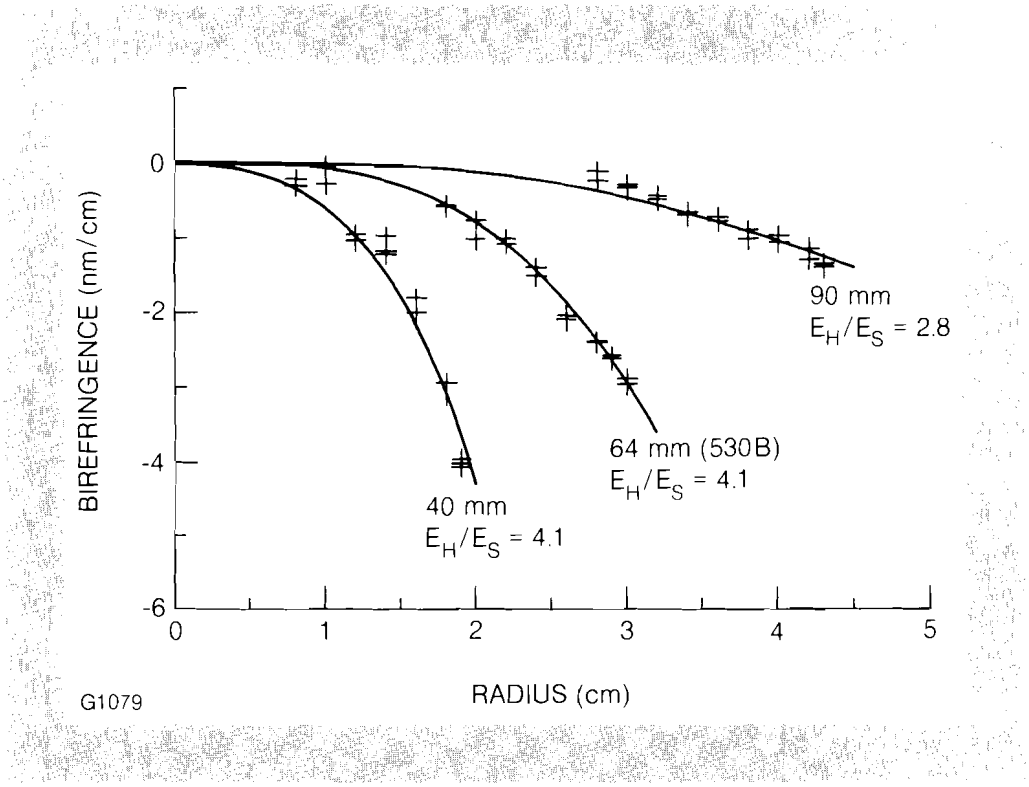

Fig. 19 Radial variation of active birefringence in various OMEGA system laser rods.

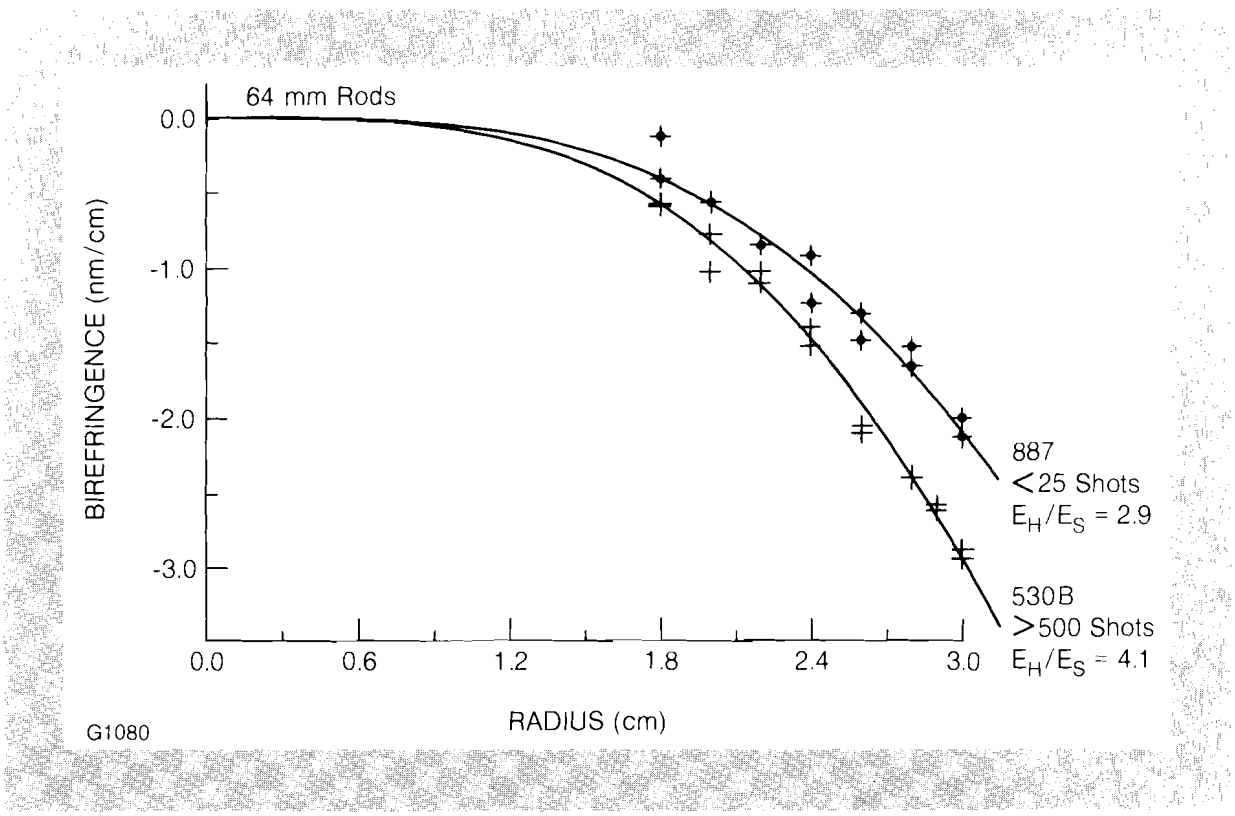

Fig. 20 Radial variation of birefringence in a used (#530B) and an unused (#887) 64-mm-diameter laser rod.

tested. The unused rod displays less birefringence than the used one. The constants of proportionality are 2.9 and 4.1 respectively. A similar difference exists between the constants of proportionality of the 90-mm and the 40-mm rods. The 90-mm rod, with approximately 350 system shots on it, reaches the best fit with a constant of proportionality of 2.8 whereas the 40-mm rod, with many shots, has a constant of 4.1. It is possible to attribute the difference to increased absorption due to solarization, but the definitive test will be to measure the birefringence of a new rod, and remeasure it after it has been subjected to several hundred system shots.

For the 64-mm rods, the one-dimensional pumping simulations predict a constant of proportionality between the stored energy density and the deposited heat of 1.9. The measurements here show 2.9 for a new rod. This difference is not totally unexpected since the simulations include Nd absorption and undoped glass absorption while they neglect absorption associated with the UV absorption edge of the glass as well as any infrared absorption. The measured active birefringence for all three-diameter rods has been incorporated into laser system modeling codes.

The OMEGA laser is an all-rod system. It consists of a driver line of four rods, one each of 16-, 30-, 40-, and 64-mm diameter. The driver is split horizontally into six beams; then each of these passes another 64-mm rod, the so-called "A" head. Each of the six beams is further split vertically, then horizontally, to yield 24 beams; each of these then passes a 64-mm and 90-mm rod.

In the cases studied here, the active birefringence in LHG-8 rods is small. Even in the 40-mm rod, the measured active birefringence leads to only a 14% reduction in transmission at rod edge through parallel polarizers. Only in the following special circumstances has it become a large effect.

The first example is from the driver-line, 40-mm stage. Originally, the beam throttle consisted of a half-wave plate located upstream of the 40-mm amplifier head which rotated the polarization of the beam through an angle 2θ (where θ is the angle between the fast axis of the plate and the transmission axis of the polarizer) so as to reject some of it on the Pockels cell polarizer following the rod. Near-field photographs which showed a square beam outline are explained by the active birefringence in the 40-mm rod. Figure 21 shows the output of the driver at full throttle (θ=0°), and at 12% output (θ=35°). At full output, there is some modulation at the beam circumference which is partially due to modulation of the input beam. At θ=35°, at locations in the rod where the input polarization happens to be oriented at 45° to the r- (radial) and theta-directions, 12% of the input beam is transmitted while 88% of the light which is orthogonally polarized due to retardation is transmitted. These two components combine linearly in the ratio of 2:1. At locations where the input polarization is parallel to either the r- or theta-directions, no retardation occurs and the 12% of the input is transmitted. This latter condition occurs at θ=70° and θ=–20° from the vertical reference and leads to minima in the transmitted intensity which we observe in the

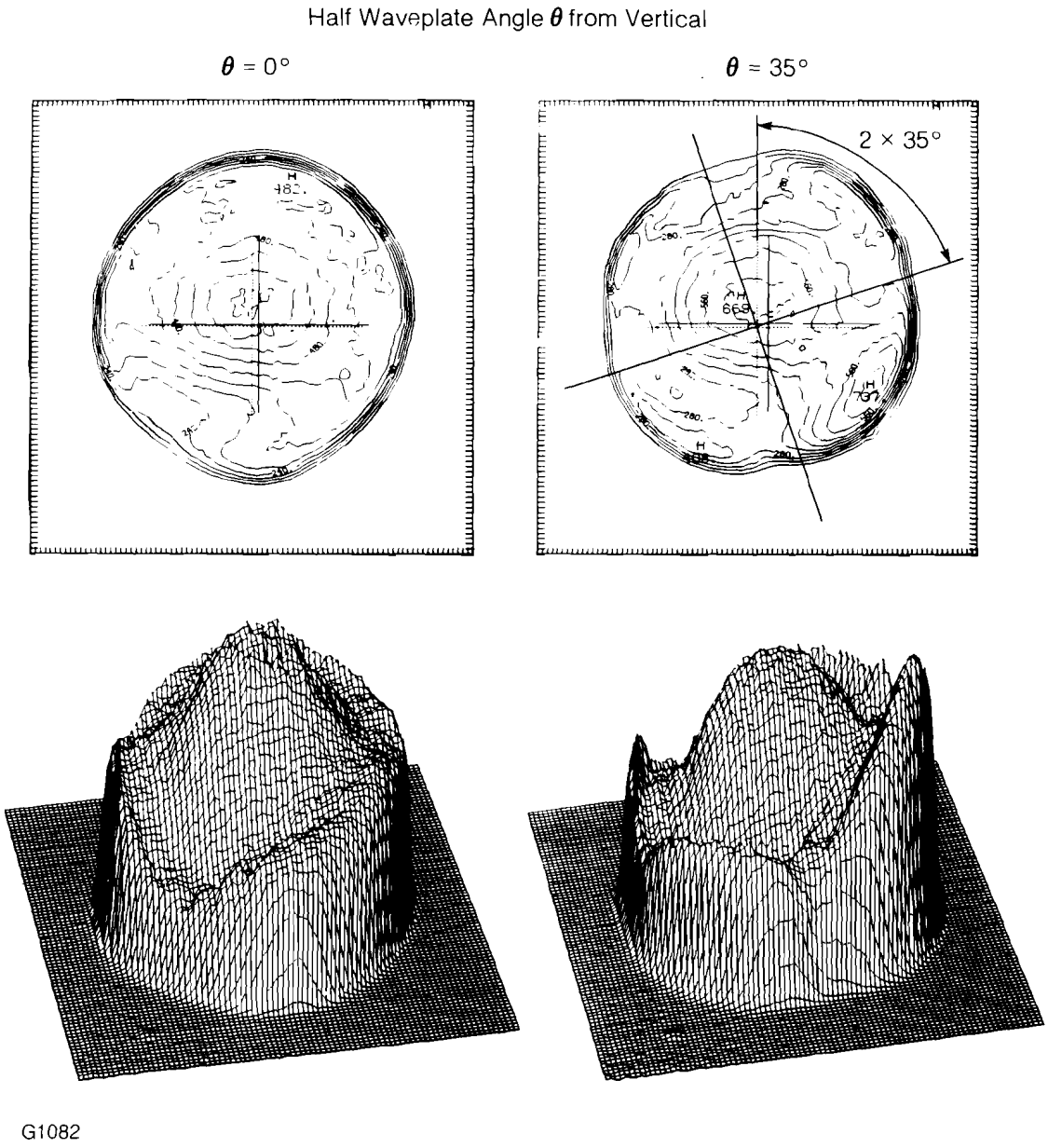

Fig. 21
Intensity distribution from the original OMEGA driver line at full throttle.

near field. Finally, if one sets the fast axis of the half-wave plate to 45°, one expects to see only the orthogonal component of the 40-mm stage again located where the input polarization to the rod is at 45° to the r- and theta-axes. This is clearly seen in Fig. 22. (Note here that the film exposure was saturating on the peak-intensity part of the beam.) The variation in the height of the four peaks is probably due to the miscentering of the beam in the rod.

The OMEGA system has since been reconfigured to eliminate this problem by locating the throttle plate further upstream in the system.

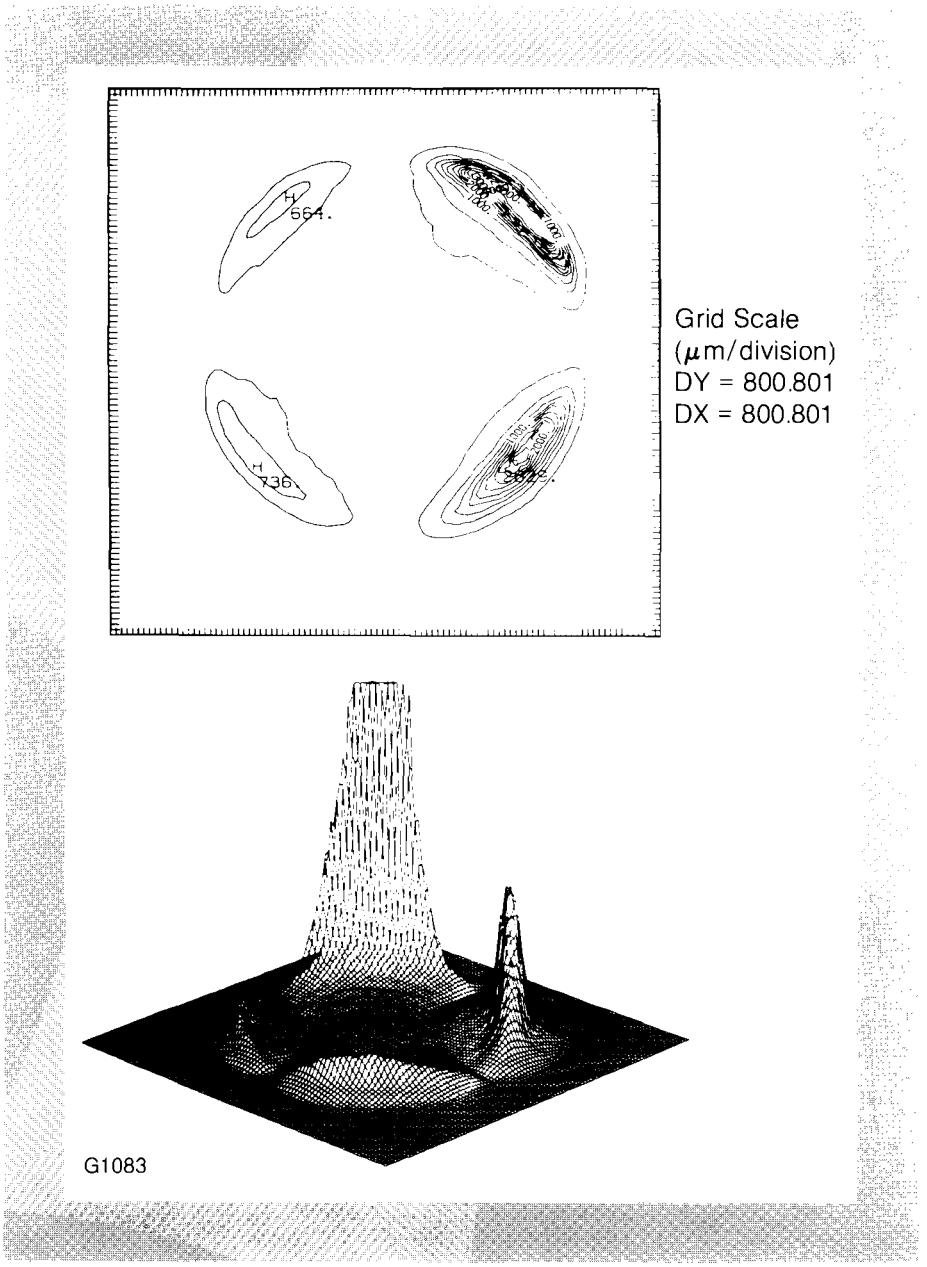

Fig. 22
Intensity distribution from the original OMEGA driver line with the throttle plate axis set at 45° to the vertical.

The second example illustrating the importance of thermal birefringence, is from a series of characterization shots performed on the system in early 1981.[3] In this particular test, the system was fired 13 times at a twelve-minute repetition rate. (Note that the system was designed to have a minimum time between shots of 30 minutes.) The stage of interest is the "A" stage, after which the beam is split (by polarizing beam splitters) into four beams. The first "up/down" split of the four-way split is shown in Fig. 23. In all beam clusters, pure left-hand circularly polarized light is injected into the 64-mm rod. Ideally, this light has an azimuthally symmetric intensity profile. The 64-mm rod in this test exhibited an inverted temperature profile and was highly birefringent because of the relatively high repetition rate. The light emerging from the rod passes a quarter-wave plate aligned with its fast axis vertical. The light emerges with a spatially varying elliptical polarization but still with

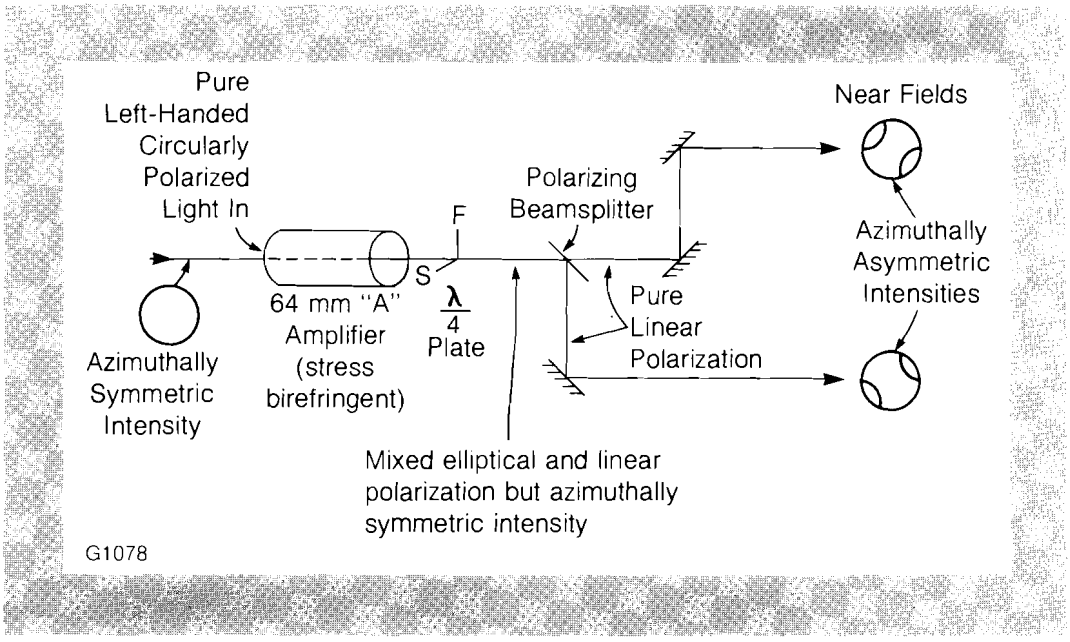

Fig. 23
Schematic layout of the OMEGA "up/down" beam-splitter system.

azimuthally symmetric intensity. If the emergent light were perfectly, linearly polarized, it would be split into identical, azimuthally symmetric beams. Since the polarization ellipses are actually distributed as shown in Fig. 24, the polarizing beam splitter splits the beam into two non-identical, non-azimuthally symmetric halves. The results of passing this beam through a vertically oriented polarizer is shown in Fig. 25. Again, the polarization ellipses (they are all straight lines) are shown. The orientation of all the lines are the same (having just passed a polarizer), but the lengths are different, indicating the relative transmission. The predicted profile of the beam includes suppression of the upper left and lower right quadrants. This is qualitatively what is observed as is shown in Fig. 26. (In Fig. 25, the beam is propagating out of the page. In Fig. 26, it is propagating into the page.) The exact beam shape will depend on the radial profile of the input beam and the temperature profile in the rod. No attempt was made to measure the birefringence of a 64-mm rod under high-repetition-rate conditions.

The lower beam is expected to be the mirror image of the upper. This is not quite what is observed, as is shown in Fig. 27. The beam has been diminished in the opposite quadrants, but significant modulation remains in the original upper left and lower right quadrants. It is not yet clear why this is, but a non-azimuthally symmetric input to the 64-mm rod is suspected.

As a result of this study, a change to circular polarization in the OMEGA driver line will be made in the near future. Work to identify other sources of azimuthal asymmetry in the system will also continue. The measured values of stress birefringence have been incorporated into the raytrace code *RAINBOW* and are being used to predict losses at polarizers.

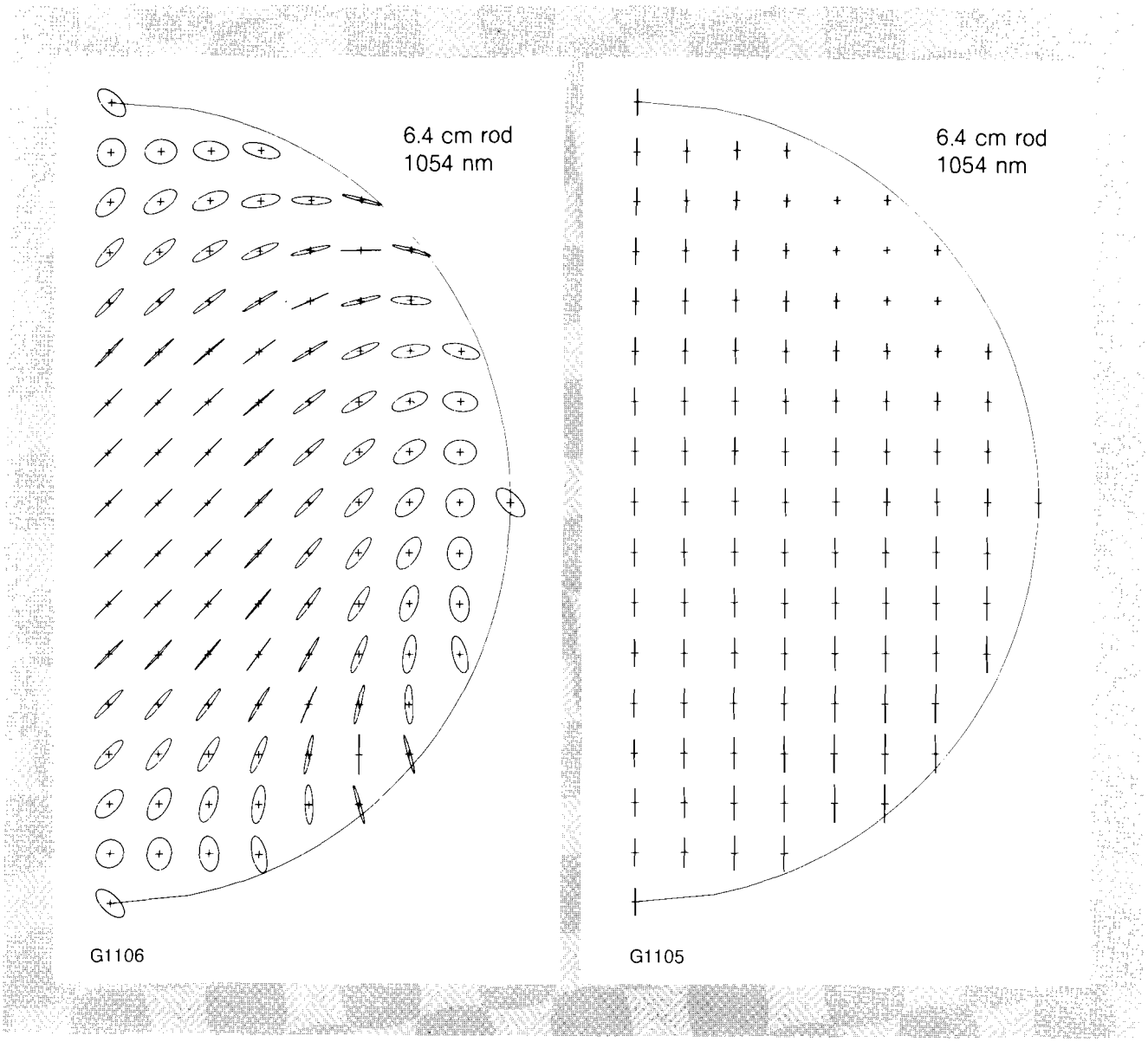

Fig. 24
Spatial distribution of polarization measured immediately after the quarter-wave plate in the "up/down" beam-splitter system (Fig. 23).

Fig. 25
Spatial distribution of polarization measured after the vertical polarizer in the "up/down" beam-splitter system (Fig. 23).

REFERENCES

1. S. Skupsky and K. Lee, LLE Report No. 137, January 1983.

2. F. W. Quelle, *Appl. Opt.* **5**, 633 (1966).

3. *LLE Review* **7**, 5 (1981).

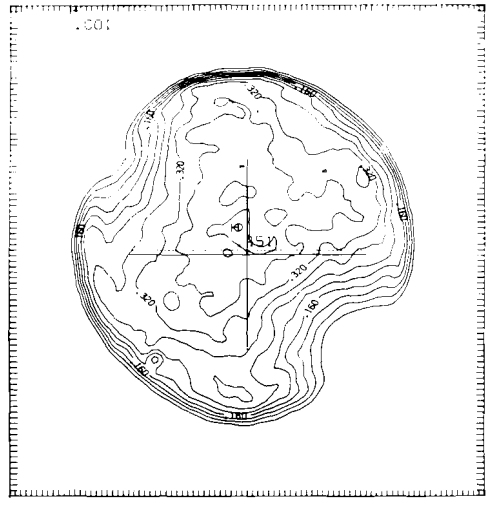

Fig. 26
Isointensity contour plot of the intensity distribution of the upper beam from the "up/down" beam-splitter system (Fig. 23). This pattern was recorded after firing 13 shots on the OMEGA system at a 12-minute-repetition rate.

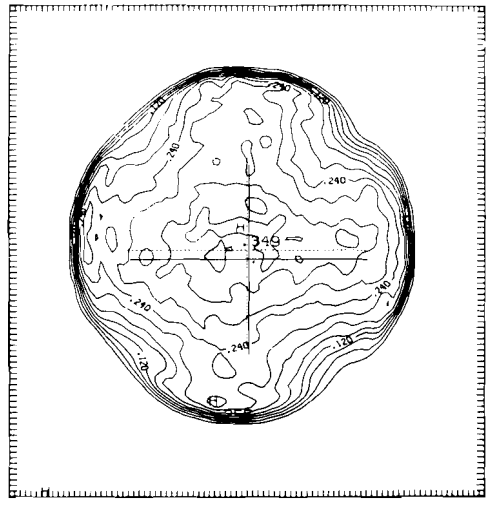

Fig. 27
Isointensity contour plot of the intensity distribution of the lower beam from the "up/down" beam-splitter system recorded at the same time as the pattern shown in Fig. 26.